

## Dendritic Branch-constrained N-Methyl-D-Aspartate Receptor-mediated Spikes Drive Synaptic Plasticity in Hippocampal CA3 Pyramidal Cells

Federico Brandalise,<sup>a,c\*</sup> Stefano Carta,<sup>b</sup> Roberta Leone,<sup>a</sup> Fritjof Helmchen,<sup>b</sup> Anthony Holtmaat<sup>a\*</sup> and Urs Gerber<sup>c†</sup>

<sup>a</sup> Department of Basic Neurosciences and the Center for Neuroscience, Centre Médical Universitaire (CMU), University of Geneva, 1211 Geneva, Switzerland

<sup>b</sup> Brain Research Institute and Neuroscience Center Zurich, University of Zurich, CH-8057 Zurich, Switzerland

<sup>c</sup> Former affiliation

**Abstract**—N-methyl-D-aspartate receptor-mediated (spikes can be causally linked to the induction of synaptic long-term potentiation (LTP) in hippocampal and cortical pyramidal cells. However, it is unclear if they regulate plasticity at a local or global scale in the dendritic tree. Here, we used dendritic patch-clamp recordings and calcium imaging to investigate the integrative properties of single dendrites of hippocampal CA3 cells. We show that local hyperpolarization of a single dendritic segment prevents NMDA spikes, their associated calcium transients, as well as LTP in a branch-specific manner. This result provides direct, causal evidence that the single dendritic branch can operate as a functional unit in regulating CA3 pyramidal cell plasticity.

*This article is part of a Special Issue entitled: Dendrites.* © 2021 The Author(s). Published by Elsevier Ltd on behalf of IBRO. This is an open access article under the CC BY-NC-ND license (<http://creativecommons.org/licenses/by-nc-nd/4.0/>).

**Key words:** dendrites, dendritic spike, plasticity, LTP, hippocampus, CA3.

### INTRODUCTION

Each neuron in the brain receives thousands of synaptic inputs on its dendrites (London and Häusser, 2005; Hawkins and Ahmad, 2016), originating from local and recurrent neuronal circuits, as well as from long-range projecting neurons. Dendrites can integrate these inputs linearly (Cash and Yuste, 1998) such that when a sufficient number are active at the same time, the summed depolarization will reach the threshold for the generation of an action potential (AP) and hence lead to transfer of information to postsynaptic targets (Cash and Yuste, 1999). However, under certain conditions, co-active inputs can result in supralinear events called dendritic spikes (dSpikes) (Spruston, 2008; Major et al., 2013). dSpikes come in various forms and are usually classified based on their duration, threshold and most importantly the type of conductance that constitutes them. Generally, dSpikes fall into three main classes: sodium (Na<sup>+</sup>) spikes (Ariav et al., 2003; Remy et al., 2009; Kim et al., 2015), calcium (Ca<sup>2+</sup>) spikes (Kampa et al., 2006; Rancz and Häusser, 2006; Suzuki and Larkum, 2017), and N-methyl-D-aspartate receptor-mediated (NMDA) spikes (Major et al., 2008, Palmer et al., 2014, Augustinaite

et al., 2014; for a comparison of the three types see also Antic et al., 2010, Stuart and Spruston, 2015). Due to the Ca<sup>2+</sup> permeability of NMDA receptors, NMDA spikes are accompanied by a fast rise in the local dendritic cytosolic Ca<sup>2+</sup> concentration (Chalifoux and Carter, 2011; Oikonomou et al., 2012; Kumar et al., 2018). In hippocampal pyramidal cells, such NMDAR-dependent, branch-specific Ca<sup>2+</sup> transients have been described both *in vitro* (Makara and Magee, 2013; Brandalise et al., 2014, Basu et al., 2016) and *in vivo* (Sheffield and Dombeck, 2015; Sheffield et al., 2017; Rashid et al., 2020). They are positively correlated with AP discharges (Makara and Magee, 2013; Grienberger et al., 2014) as well as synaptic long-term potentiation (LTP) (Brandalise et al., 2016). However, despite the close relationship between local NMDA spikes and the induction of LTP in various brain areas (Gambino et al., 2014; Cichon and Gan, 2015; Bono and Clopath, 2017; Topolnik and Camiré, 2019), causal evidence is still lacking. The difficulty in establishing a causal link is in part due to the fact that NMDA spikes as measured at the soma may originate from multiple dendritic branches and hence affect plasticity processes globally. To determine the causal relationship between locally generated NMDA spikes and subsequent plasticity it is necessary to elicit and interrogate them locally at single dendritic branches.

Here, we use simultaneous electrical recordings from the soma and dendrite of CA3 pyramidal neurons, combined with Ca<sup>2+</sup> imaging, to evaluate the role of

\*Correspondence to: Federico Brandalise, Department of Basic Neurosciences and the Center for Neuroscience, Centre Médical Universitaire (CMU), University of Geneva, 1211 Geneva, Switzerland.

E-mail address: fedebio86@gmail.com (F. Brandalise).

† Currently retired.

64 locally generated NMDA spikes in synaptic plasticity.  
65 Local dendritic hyperpolarization prohibits the generation  
66 of branch-selective NMDA spikes and  $\text{Ca}^{2+}$  events, and  
67 prevents synaptic LTP. When NMDA spikes are  
68 generated in multiple branches, local hyperpolarization  
69 prevents  $\text{Ca}^{2+}$  events and LTP only in the recorded  
70 dendrite. Together, these data underscore a powerful  
71 causal relationship between locally triggered NMDA  
72 spikes and the induction of synaptic LTP.

## 73 EXPERIMENTAL PROCEDURES

### 74 Preparation of hippocampal slice cultures

75 All experiments described here were performed in rat  
76 organotypic slice cultures (Brandalise and Gerber, 2014;  
77 Brandalise et al., 2016), following a protocol approved  
78 by the Veterinary Department of the Canton of Zurich (ap-  
79 proval ID 81–2014). The cultures were prepared from 6-  
80 day-old Wistar rats using the Gähwiler method  
81 (Gähwiler, 1981), which results in a quasi-monolayer of  
82 cells that facilitates dendritic imaging. Transverse slices  
83 were obtained (400  $\mu\text{m}$ ) and placed to coverslips with  
84 clotted chicken plasma. These were stored in sealed test  
85 tubes with serum-containing medium and maintained in a  
86 moving incubator at 36 °C for 21–28 days.

### 87 Patch-clamp recordings

88 Hippocampal slice cultures were mounted in an  
89 electrophysiological recording chamber under a 2-  
90 photon laser scanning microscope (2PLSM), which  
91 allows simultaneous electrophysiological recordings and  
92 calcium imaging. Slice cultures were maintained in an  
93 external recording solution (pH 7.4) containing (in mM):  
94 137 NaCl, 2.7 KCl, 11.6  $\text{NaHCO}_3$ , 0.4  $\text{NaH}_2\text{PO}_4$ , 2  
95  $\text{CaCl}_2$ , 2  $\text{MgCl}_2$ , 5.6 D-glucose and 0.001% phenol red  
96 to monitor pH. All experiments were performed at 34 °C.  
97 CA3 pyramidal cells were simultaneously recorded at  
98 the soma and a first-order dendritic branch using whole-  
99 cell recording patch pipettes. Somatic pipettes had a  
100 resistance between 5 and 7  $\text{M}\Omega$  and dendritic pipettes  
101 between 9 and 11  $\text{M}\Omega$ . Both somatic and dendritic patch  
102 pipettes were filled with internal solution (pH 7.2)  
103 containing (in mM): 135 K-gluconate, 5 KCl, 10 HEPES,  
104 5 phosphocreatine, 2 MgATP, 0.4 NaGTP and 0.07  
105  $\text{CaCl}_2$ . For visualization of dendrites and calcium  
106 signals, cell filler Alexa Fluor 495 (Alexa-495; 10  $\mu\text{M}$ )  
107 and the calcium dye Fluo-5F (100  $\mu\text{M}$ ) (both from  
108 Molecular Probes) were added to the internal solution.  
109 To prevent spontaneous APs or  $\text{Na}^+$  dendritic spikes,  
110 QX-314 (500 nM) was included in the recording pipette.  
111 To reduce GABA<sub>A</sub> mediated responses, picrotoxin  
112 (1 mM) was included in the somatic electrode. Average  
113 resting membrane potential (RMP) of the recorded cells  
114 was  $-63.8 \pm 4.6$  mV (mean  $\pm$  s.e.m.;  $n = 14$ ). Voltage  
115 commands were corrected for the liquid junction  
116 potential (8.3 mV). Stimulation strength was calibrated to  
117 keep the postsynaptic responses below the AP  
118 threshold (amplitude  $5.6 \pm 1.1$  mV for rCA3;  $7.8$   
119  $\pm 1.6$  mV for MF; measured at the soma;  $n = 14$ ).

### Stimulation paradigm

To activate rCA3 synaptic inputs in the apical dendritic  
tree, a theta-glass electrode was placed in the stratum  
radiatum of CA3, and to activate MF inputs, an  
electrode was placed in the dentate gyrus. The theta  
glass electrode (tip diameter = 5–20  $\mu\text{m}$ ) was filled with  
extracellular solution. Electrodes were located as close  
as possible (10–20  $\mu\text{m}$ , see asterisks in Figs. 1A and  
2A) to the apical dendrite in different locations until  
supralinear events were detected (upon pairing with MF  
inputs). The input timing dependent plasticity (ITDP)  
protocol consisted of 60 pairings at 0.1 Hz, with the MF  
inputs activated after the rCA3 inputs with a 10-ms  
delay. Stimulation intensities were set such that  
postsynaptic potentials remained below the action  
potential threshold. ITDP protocol 1 (ITDP1) included in  
addition to the rCA3-MF pairings a 25-ms long  
hyperpolarizing square current injection pulse starting at  
MF-stimulation onset ( $\sim 0.1$  nA, resulting in  $\sim 6$  mV drop  
in membrane potential). ITDP protocol 2 (ITDP2) is  
identical to ITDP protocol 1 but without the  
hyperpolarizing square pulse. After accessing the cell  
with the somatic electrode, but before the ITDP  
protocol, part of the apical dendritic arbor was scanned  
to locate active branches by applying a few cycles of  
rCA3-MF stimulation pairings ( $\sim 5$  on average; with an  
interval of 1 minute between stimulations in each FOV).  
Of the final two FOVs, one was centered on active  
branches, the other on inactive branches.

### NMDA spike analysis

To identify the supralinear events (representing NMDA  
spikes) in the voltage recordings of each ITDP protocol,  
we first normalized all 60 traces to the amplitude of the  
baseline-evoked rCA3 EPSP. A histogram of the  
maximum amplitudes revealed a bimodal distribution.  
The traces representing the EPSP amplitudes that  
belonged to the first gaussian were considered linear  
responses, whereas those of the second gaussian were  
classified as NMDA spikes (for a more detailed  
explanation of the analysis see Brandalise et al., 2016).  
The NMDA spike probability was calculated as the ratio  
of the traces that were classified as NMDA spikes over  
the total number of traces (60). The normalized NMDA  
spike amplitude was represented as the percent increase  
from the amplitude of the mean linear response.

### Two-photon $\text{Ca}^{2+}$ imaging

For  $\text{Ca}^{2+}$  imaging, neurons were dialyzed with internal  
solution containing Fluo-5F (100  $\mu\text{M}$ ) and Alexa-495  
through the dendritic recording pipette for at least  
10 min before imaging was performed. Neurons were  
imaged using a 2PLSM (Scientifica) equipped with a Ti:  
sapphire laser (Tsunami, Spectra Physics) tuned to  
840 nm and a 40x water-immersion objective lens (0.8  
NA, Olympus). The laser power under the objective was  
typically between 10 and 15 mW. Emitted fluorescence  
was detected using two photomultiplier tubes, and  
spectrally separated using 525/50 nm (green channel)

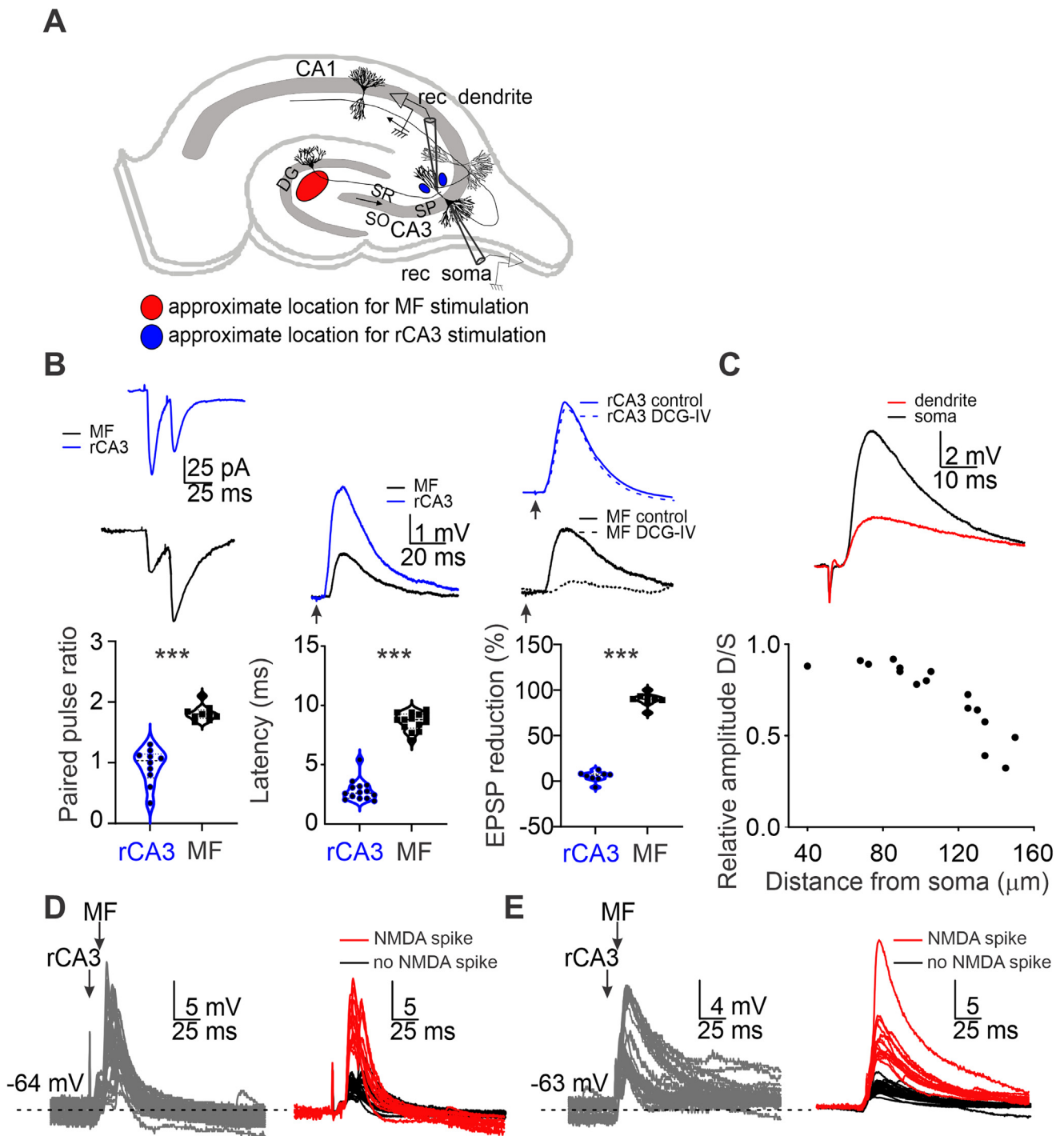


**Fig. 1.** Experimental configuration and differentiation between MF and rCA3 inputs. **(A)** Schematic depicting the positions of the recording and stimulation electrodes. The recording electrodes were placed in the stratum pyramidale (SP) and in the stratum radiatum (SR), respectively. Two stimulating electrodes were placed in the CA3 SR (blue) and in the dentate gyrus (DG; red) to excite CA3r and MF input, respectively. **(B)** Representative current traces of a paired stimulation with a 50-ms interval between the two pulses with the pooled data plots. Each point represents a recorded neuron. MF inputs to CA3 PCs evoke significant paired-pulse facilitation whereas rCA3 stimulation induce either paired-pulse facilitation or depression. The latency between the stimulation artefact and the EPSP is longer when stimulating MF as opposed to rCA3. Bath perfusion of DCG-IV ( $2 \mu\text{M}$ ), an mGlu2R agonist, significantly reduces mossy fiber responses but not rCA3 responses. **(C)** The ratio of dendritic and somatically recorded EPSP amplitudes (D/S) upon MF stimulation, as a function of the distance of the dendritic recording pipette from soma. The negative relationship indicates that the EPSPs are passively filtered along the dendrites. **(D, E)** Two dendritic recordings in which rCA3 and MF input stimulation with 10-ms delays (grey traces) frequently results in supralinear events (red traces) that can be distinguished from linear events (black traces) after normalization to the rCA3 EPSPs (see Methods). (For interpretation of the references to colour in this figure legend, the reader is referred to the web version of this article.)

177 and 620/60 nm (red channel) emission filters. Scanning  
178 and image acquisition were controlled by HelioScan  
179 software (Langer et al., 2013). Recordings of Fluo-5F fluo-  
180 orescence ( $\text{Ca}^{2+}$ ) transients were acquired at a 10 Hz  
181 frame rate with the imaging fields ( $100 \times 100$  pixels, at  
182 a  $0.3 \mu\text{m}/\text{pixel}$  resolution) encompassing several  
183 dendrites.

184 In order to record  $\text{Ca}^{2+}$  transients in several branches  
185 for each experiment, 2 FOVs were imaged alternately  
186 over the 60 pairings of the ITDP protocols, resulting in  
187 data sets consisting of 30 responses for each FOV. This  
188 was preferred over simultaneous data acquisition from  
189 multiple FOVs as this would have resulted in images  
190 with insufficient resolution for detailed analysis. We  
191 have previously found no change in the probability of  
192 evoking an NMDA spike over the time course of the 60  
193 pairings (Supplementary Fig. 4 in Brandalise and  
194 Gerber, 2014).

195 At the end of each experiment, z-stacks of the  
196 fluorescently labelled cells were acquired to verify that  
197 the recorded neurons were indeed CA3 pyramidal cells.  
198 The z-stacks were also used to estimate the distance  
199 between the somatic and dendritic recording electrode.  
200 Data were analyzed with NIH ImageJ and Igor Pro  
201 (WaveMetrics) software. In ImageJ, dendritic segments  
202 were manually drawn as regions of interest (ROIs).  
203  $\text{Ca}^{2+}$  signals were expressed as  $\Delta F/F = (F - F_0)/F_0$   
204 where  $F$  and baseline  $F_0$  represent mean fluorescence  
205 values in an ROI. A  $\text{Ca}^{2+}$  transient was considered as a  
206 signal when its amplitude was greater than two times  
207 the standard deviation (s.d.) of the noise ( $\sim 7\%$ ).  $\text{Ca}^{2+}$   
208 transients that were temporally locked to the electrical  
209 stimulation were temporally integrated over a 2-s post-  
210 stimulus window, using custom-written scripts in  
211 MATLAB (units of ‘%’; after subtraction of the mean  
212  $\Delta F/F$  in a 1-s pre-stimulus baseline window).

## 213 Statistical analysis

214 All data are expressed as the mean  $\pm$  s.e.m. A total  
215 amount of 7 rats were used for this work. From each  
216 brain it was possible to obtain  $\sim 10$ – $15$  organotypic  
217 slices. 2 recordings per rat were included in the data

set, and each recording was from a different slice 218  
culture. No data sets were excluded from analysis. 219  
Statistical analyses were performed using Origin 2016 220  
(OriginLab) as well as GraphPad PRISM 2019. 221  
Statistical significance was calculated using non- 222  
parametric tests (Wilcoxon matched-pairs signed rank 223  
test for paired comparisons; Kruskal–Wallis test for 224  
comparison between more than two groups). 225

## Data availability

The authors declare that the experimental results 226  
supporting the findings are included in the article and 227  
are available upon reasonable request. 228  
229

## RESULTS

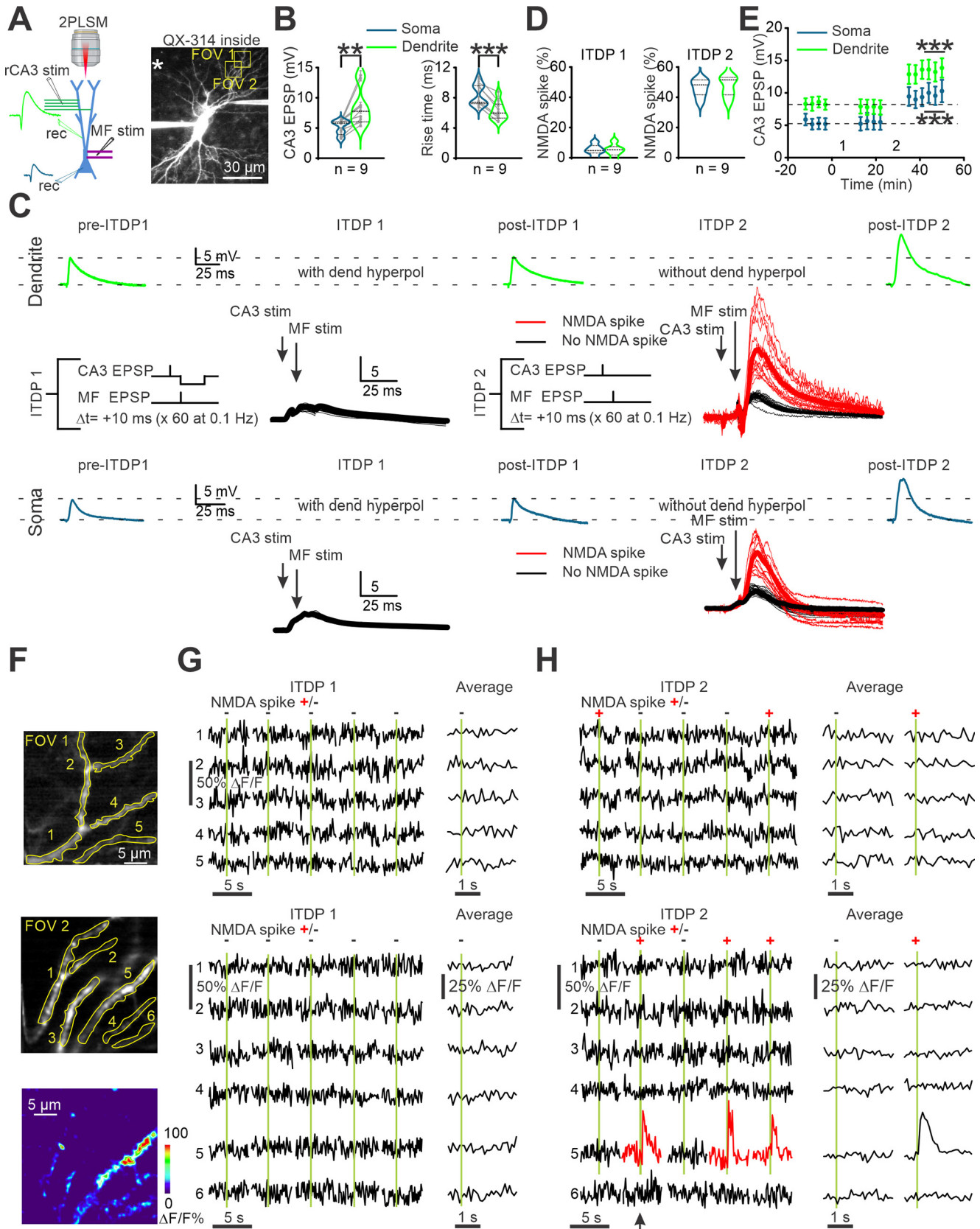
### Locally generated NMDA spikes are sufficient and necessary for rCA3 and MF pairing-induced LTP

Hippocampal CA3 pyramidal cells (PCs) receive 233  
excitatory input in a spatially segregated manner from 234  
mossy fibers (MFs) on the initial portions of apical and 235  
basal dendrites, from recurrent axons from neighboring 236  
CA3 pyramidal cells (rCA3s) on more medially located 237  
apical and basal dendrites, and from perforant-path 238  
axonal fibers originating in the entorhinal cortex on distal 239  
portions of the apical dendrites (Fig. 1A) (Amaral and 240  
Witter, 1989). Here, we performed dual electrical record- 241  
ings from the soma and dendrites of single CA3 PCs in 242  
organotypic slice cultures of rat hippocampus, while 243  
sequentially stimulating rCA3 and MF afferents. By using 244  
theta-glass electrodes, we aimed at focal stimulation of 245  
rCA3 afferents close to CA3 PC dendrites (see Methods). 246  
This protocol has previously been shown to generate 247  
NMDA spikes and synaptic plasticity (Brandalise and 248  
Gerber, 2014; Brandalise et al., 2016). MF and rCA3 249  
synapses onto CA3 PCs have been shown to be function- 250  
ally distinct (Debanne et al., 1995; Kamiya et al., 1996; 251  
Salin et al., 1996; Mori et al., 2004). Therefore, to verify 252  
that we could independently stimulate these two inputs, 253  
we evaluated the properties of EPSPs generated by 254  
either the MF or rCA3 stimulation electrode. As compared 255  
to rCA3 inputs, MF inputs showed longer response onset 256

**Fig. 2.** Local dendritic hyperpolarization prevents focal stimulation-evoked NMDA spikes and LTP. (A) Left, schematic of the dendritic and somatic patch-clamp recordings in CA3 cells, and the paired stimulation of rCA3 and MF inputs. rCA3 axons are focally stimulated near the dendritic electrode, which predominately activates synapses on the recorded dendrite. Right, a CA3 pyramidal neuron filled with Fluo-5F and Alexa-495, imaged in the Alexa channel, which visualizes the soma, dendrites as well as the somatic and dendritic electrodes. FOV 1 and 2 refer to the examples provided in (F–H). (B) Focal stimulation of rCA3 inputs results in larger amplitudes and shorter rise times of the EPSPs in the dendritic (green) as compared to the somatic (blue) recordings ( $P = 0.005$ ;  $P = 0.004$ ). (C) Protocols for input timing dependent plasticity (ITDP), consisting of rCA3-EPSPs baseline recordings (pre-ITDP) followed by 60 paired rCA3 and MF stimulations at 0.1 Hz, and another series of rCA3-EPSP recordings (post-ITDP), both at the dendrite (green) and the soma (blue). During the first series of pairings (ITDP 1) a hyperpolarizing step was delivered through the dendritic recording pipette immediately following mossy fiber stimulation. In the second series of pairings (ITDP 2) this hyperpolarization step was omitted. During ITDP 1, only linear responses (black traces) could be detected at the soma and dendrite, and the post-ITDP 1 rCA3 EPSP amplitude was similar to the pre-ITDP 1 EPSP. During ITDP2, NMDA spikes (red traces) were also detected both at the soma and the dendrite, and the post-ITDP2 rCA3 EPSP amplitude was increased. (D) Pooled data for the percentage of paired stimulations that evoked NMDA spikes during ITDP 1 and ITDP 2 at the soma (blue) or at the dendrites (green). (E) Pooled data for the rCA3 EPSP amplitudes normalized to baseline after ITDP 1 (1) and ITDP 2 (2), indicating a significant increase after ITDP 2 ( $P = 0.0004$ ). (F) Top, examples of pairing-evoked  $\text{Ca}^{2+}$  transients in two portions of the dendritic tree (FOV 1 and FOV 2) of the recorded cell. The lines delimit the individual dendritic branches in which the transients were analyzed. Bottom, the Fluo-5F  $\Delta F/F$  fluorescence change for one pairing trial (arrow in (H)). (G) Example  $\text{Ca}^{2+}$  transients from the ROIs in (F), recorded during 5 representative consecutive pairings (green bars) during ITDP 1. Trials with linear (“–”) and supralinear (“+”) EPSP summation are indicated.  $\text{Ca}^{2+}$  transients for FOV1 and FOV2 were averaged separately for linear and supralinear trials. (H) Same as (H) but during ITDP 2. (For interpretation of the references to colour in this figure legend, the reader is referred to the web version of this article.)

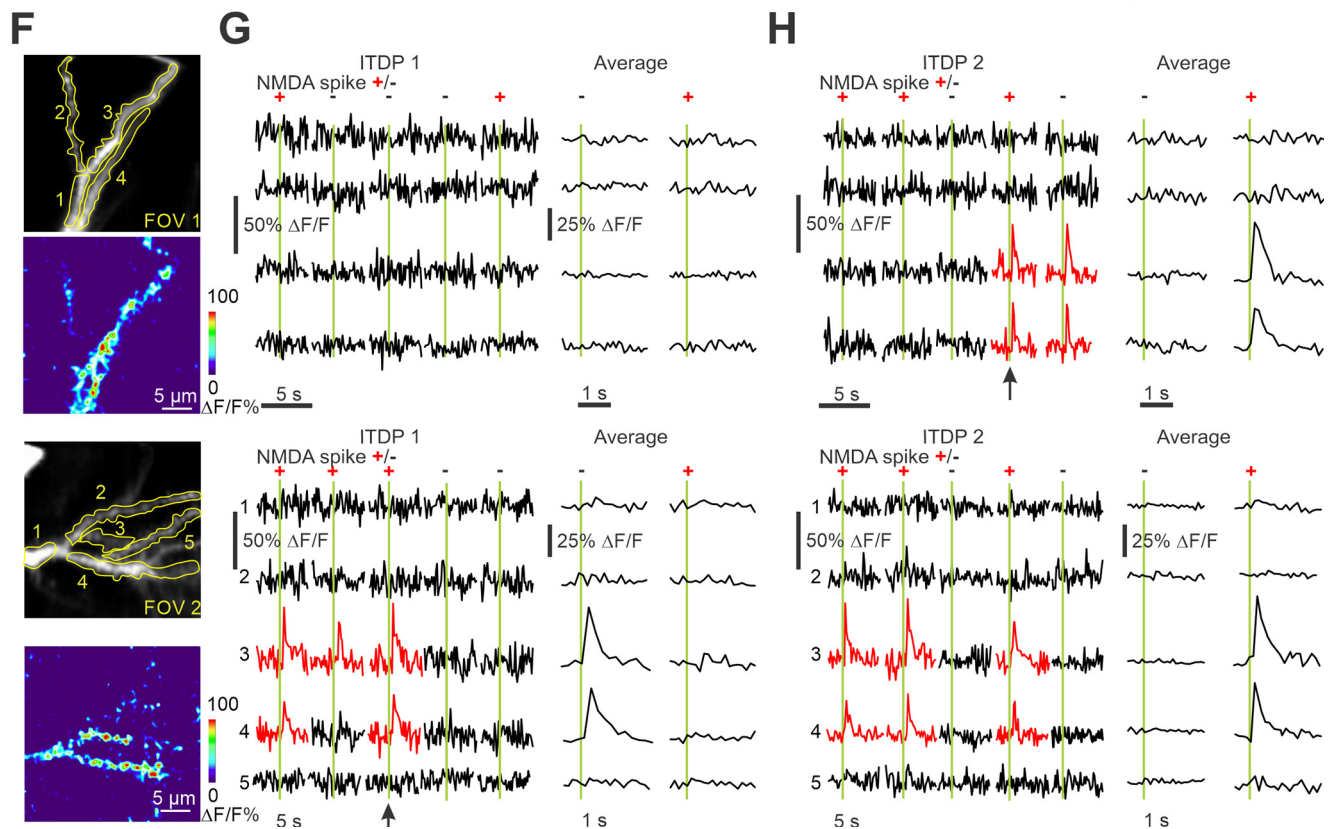
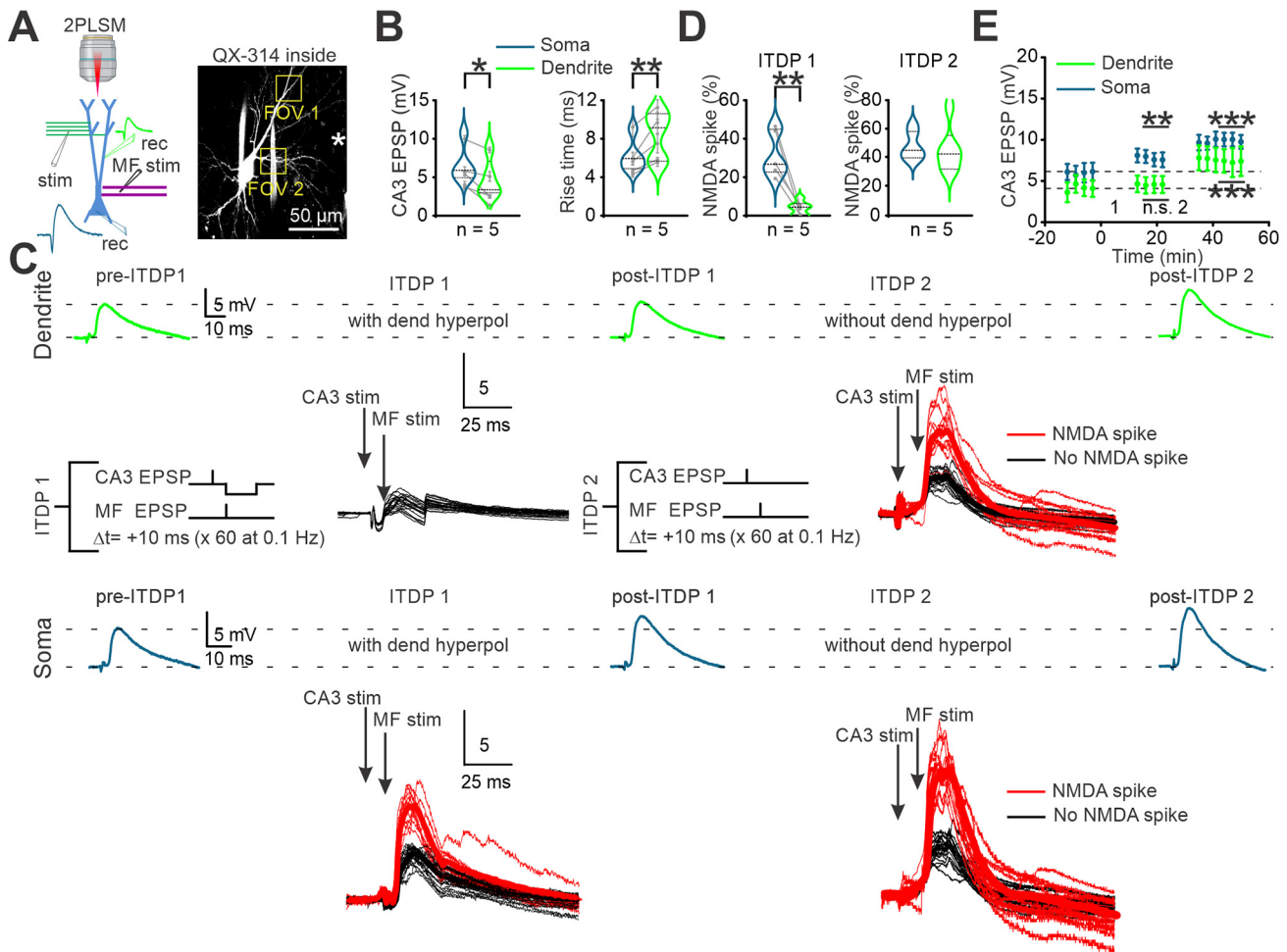
257 latencies ( $8.4 \pm 0.2$  ms,  $n = 8$  versus  $2.8 \pm 0.2$  ms,  
258  $n = 8$ ;  $P < 0.001$ ), paired pulse facilitation ( $1.81 \pm 0.1$   
259 for MF,  $n = 8$  versus  $0.94 \pm 0.1$   $n = 8$ ;  $P < 0.001$ ) and

260 much stronger sensitivity to DCG-IV, a selective mGluRII  
261 blocker (percentage of reduction  $95.3 \pm 2.3\%$ ,  $n = 8$ ,  
262  $P < 0.001$  versus CA3r percentage of reduction 12



6

F. Brandalise et al. / Neuroscience xxx (2021) xxx–xxx



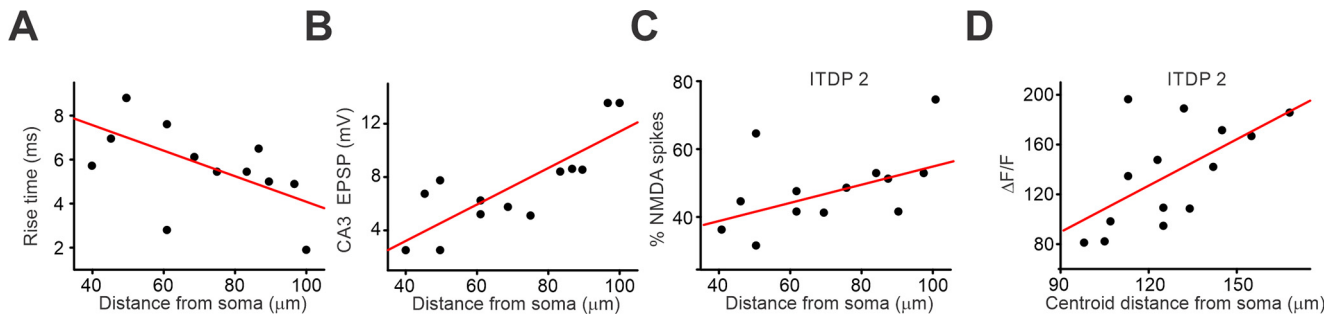


**Fig. 4.** Correlation of rCA3-evoked EPSPs and MF-rCA3-evoked NMDA spikes with the distance along the dendritic tree. Rise time (**A**) and amplitude (**B**) of rCA3 EPSPs as a function of the distance of the dendritic electrode location from the soma. Percentage of NMDA spikes (**C**) and amplitude of the branch-constrained calcium transients detected during the ITDP 2 protocol (**D**) as a function of the distance of the dendritic electrode location from the soma.

± 1%,  $n = 8$ ,  $P = 0.19$ ; Fig. 1B). These distinct characteristics agree with previous findings (Brandalise and Gerber, 2014) and indicate that our electrode configuration provided selective access to either synaptic pathway. In addition, we found that MF-mediated depolarizations could passively spread to the medial portion of the dendrites as could be measured by the dendritic recording pipette (Fig. 1C), suggesting that MF inputs are able to interact with rCA3 inputs at the dendritic level. Indeed, the combined sequential stimulation of rCA3 and MF with a 10-ms delay induced supralinear events in a substantial fraction of the trials (red traces in Fig. 1D; see methods for classification criteria), which were previously shown to correspond to NMDA spikes (Brandalise and Gerber, 2014; Brandalise et al., 2016).

Before applying any plasticity protocols (Figs. 2 and 3) we first recorded baseline excitatory postsynaptic potentials (EPSPs) evoked by rCA3 stimulation alone for at least 10 mins (Fig. 2A, B). Since rCA3 axons make synaptic contacts mainly with secondary order

dendrites, which branch off from the first order branches that we recorded from (Fig. 2A), the stimulation typically resulted in a greater amplitude and a faster rise time of the postsynaptic response at the dendritic recording electrode (green) as compared to the somatic electrode (blue) (Fig. 2B; amplitude:  $8.4 \pm 3.1$  mV for the dendrite;  $5.0 \pm 1.2$  mV for the soma;  $P = 0.005$ ; rise time:  $6.4 \pm 0.4$  ms for the dendrite;  $8.5 \pm 0.5$  ms for the soma;  $P = 0.004$ ;  $n = 9$ ). The dendritic rise times inversely correlated with the pipette's distance from the soma ( $r = 0.63$ ; Fig. 4A). Similarly, the amplitude of the dendritically recorded rCA3 EPSPs correlated with the distance from the soma ( $r = 0.80$ ; Fig. 4B). These data confirm that the electrotonic distance of the recording pipette to the rCA3 synaptic inputs decreases when the recordings are located closer to the apical dendritic tufts (Brandalise and Gerber, 2014).

Then we applied two input timing dependent plasticity (ITDP) protocols (Dudman et al., 2007) of 60 rCA3-MF paired stimuli at 0.1 Hz to evaluate the role of dendritic

**Fig. 3.** Local dendritic hyperpolarization does not prevent stimulus-evoked NMDA spikes and LTP in branches other than the recorded dendrite. (**A**) Left, schematic of the dendritic and somatic patch-clamp recordings in CA3 cells, and the paired stimulation of rCA3 and MF inputs. rCA3 axons distant from the recording electrode are stimulated, which predominantly activates synapses that are not located on the recorded dendrite. Right, a CA3 pyramidal neuron filled with Fluo-5F and Alexa-495, imaged in the Alexa channel, which visualizes the soma, dendrites as well as the somatic and dendritic electrodes. FOV 1 and 2 refer to the examples provided in (F–H). (**B**) distant stimulation of rCA3 inputs results in smaller amplitudes and longer rise times of the EPSPs in the dendritic (green) as compared to the somatic (blue) recordings ( $P = 0.01$ ,  $P = 0.007$ ). (**C**) Protocols for input timing dependent plasticity (ITDP), consisting of rCA3-EPSPs baseline recordings (pre-ITDP) followed by 60 paired rCA3 and MF stimulations at 0.1 Hz, and another series of rCA3-EPSP recordings (post-ITDP), both at the dendrite (green) and the soma (blue). During the first series of pairings (ITDP 1) a hyperpolarizing step was delivered through the dendritic recording pipette immediately following mossy fiber stimulation. In the second series of pairings (ITDP 2) this hyperpolarization step was omitted. During both ITDP 1 and ITDP 2, linear responses (black traces) and NMDA spikes (red traces) could be detected at the soma and dendrite. For both protocols, the post-ITDP rCA3 EPSPs amplitudes were increased at the soma, but only for ITDP 2 at the dendrite. (**D**) Pooled data for the percentage of paired stimulations that evoked NMDA spikes during ITDP 1 and ITDP 2 at the soma (blue) or at the dendrites (green) (**E**) Pooled data for the rCA3 EPSP amplitudes normalized to baseline after ITDP 1 (1) and ITDP 2 (2), indicating a significant increase after ITDP 1 and 2 (**F**) Top images, examples of pairing-evoked  $\text{Ca}^{2+}$  transients in two portions of the dendritic tree (FOV 1 and FOV 2) of the recorded cell. The lines delimit the individual dendritic branches in which the transients were analyzed. Bottom images, the Fluo-5F  $\Delta F/F$  fluorescence change for one pairing trial (arrows in (G, H)). (**G**) Example  $\text{Ca}^{2+}$  transients from the ROIs in (F), recorded during 5 representative consecutive pairings (green bars) during ITDP 1. Trials with linear (“–”) and supralinear (“+”) EPSP summation are indicated.  $\text{Ca}^{2+}$  transients for FOV1 and FOV2 were averaged separately for linear and supralinear trials. (**H**) Same as (H) but during ITDP 2. (**D**) Pooled data for the percentage of NMDA spikes during ITDP 1 and ITDP 2 both in the soma (blue) and in the dendrites (green). (**E**) Plots of EPSP time course. (**F**) Same CA3 pyramidal neuron labelled with Fluo-5F (**F**) Fluorescence measurements to detect pairing-induced  $\text{Ca}^{2+}$  transients were obtained in 4 ROIs in FOV 1 and 5 ROIs in FOV 2 for different portion of apical dendritic branches. Middle and bottom image shows localized Fluo-5F  $\Delta F/F$  fluorescence change for one pairing trial (indicated by a black arrow in (H) or (I)). (**H**) Example  $\text{Ca}^{2+}$  transients from ROIs selected in (G), recorded during 5 representative consecutive pairings in ITDP 1 (green bars). Trials with linear (“–”) and supralinear (“+”) EPSP summation are indicated.  $\text{Ca}^{2+}$  transients for FOV1 and FOV2 were averaged separately for linear and supralinear trials. (For interpretation of the references to colour in this figure legend, the reader is referred to the web version of this article.)

303 NMDA spikes in the induction of LTP at rCA3 synapses  
304 (Fig. 2C) (Brandalise et al., 2016). In the first protocol  
305 (ITDP1) we attempted to block NMDA spikes by applying  
306 hyperpolarizing current in the dendrite, whereas they  
307 were allowed to occur in the second (ITDP2). After each  
308 series of pairings, EPSPs evoked by only rCA3 stimulation  
309 were measured (post-ITDP EPSPs) and compared  
310 to the pre-ITDP EPSPs to assess the level of LTP. To rule  
311 out a possible contribution of spontaneous APs or den-  
312 dritic  $\text{Na}^+$  spikes during the protocol (Golding and  
313 Spruston, 1998), QX-314 (500  $\mu\text{M}$ ) was included in the  
314 dendritic recording pipettes.

315 We hypothesized that by hyperpolarizing the recorded  
316 dendrite we would reduce the opening of the voltage-  
317 dependent NMDA receptor channels mainly locally in  
318 this dendritic compartment and thereby prevent the  
319 triggering of NMDA spikes. Indeed, the negative current  
320 injection applied during ITDP1 ( $\sim 0.1\text{nA}$  for 25 ms,  
321 resulting in  $\sim 6\text{mV}$  drop in membrane potential),  
322 provided simultaneously with the MF stimulation, almost  
323 entirely prevented the generation of NMDA spikes at  
324 both the dendritic compartment (fraction of pairing  
325 stimuli with non-linear events:  $4.8 \pm 1.6\%$ ,  $n = 9$ ) and  
326 the soma ( $4.0 \pm 1.4\%$ ,  $n = 9$ ) (Fig. 2C, D). The  
327 amplitude of the rCA3 EPSPs was not affected by the  
328 ITDP1 protocol (soma:  $5.2 \pm 0.1\text{mV}$  pre-ITDP1,  $5.5$   
329  $\pm 0.1\text{mV}$  post-ITDP1,  $P = 0.4$ ,  $n = 9$ ; dendrite:  $7.7$   
330  $\pm 0.2\text{mV}$  pre-ITDP1,  $7.8 \pm 0.1\text{mV}$  post-ITDP1,  
331  $P = 0.7$ ,  $n = 9$ ; Fig. 2D, E).

332 The ITDP2 pairing protocol, for which the same  
333 stimulation intensities were used as in ITDP1 but the  
334 hyperpolarization step was omitted, successfully evoked  
335 NMDA spikes in a considerable fraction of the rCA3-MF  
336 pairings, significantly higher compared to ITDP1 and  
337 visible at both the dendrite ( $49.5\% \pm 3.5\%$ ,  $P = 0.001$   
338 vs ITDP1,  $n = 9$ ), and the soma, albeit with a  
339 dampened amplitude ( $48.6 \pm 3.4\%$ ,  $P = 0.002$  vs  
340 ITDP1,  $n = 9$ ) (Fig. 2C, D). The fraction of trials that  
341 produced NMDA spikes (recorded at the dendrite)  
342 increased with the distance of the recording pipette to  
343 the soma ( $r = 0.53$ ; Fig. 4C), suggesting that they are  
344 generated locally in the more medial portions of the  
345 dendritic tree where the rCA3 synapses are located. In  
346 contrast to ITDP1, ITDP2 caused significant increase in  
347 the rCA3 EPSP amplitude at the dendritic compartment  
348 ( $7.8 \pm 0.1\text{mV}$  pre-ITDP2;  $13.4 \pm 0.4\text{mV}$  post-ITDP2,  
349  $P = 0.0004$ ,  $n = 9$ ) as well as at the soma ( $5.5$   
350  $\pm 0.1\text{mV}$  pre-ITDP2;  $9.6 \pm 0.5\text{mV}$  post-ITDP2,  
351  $P = 0.0001$ ,  $n = 9$ ) for the whole duration of the  
352 recordings after ITDP2 (up to 20 min). This data  
353 confirms our previous observation that the repeated  
354 sequential pairing of MF and rCA3 inputs selectively  
355 drives LTP of the rCA3 inputs (and not of MF inputs;  
356 Brandalise and Gerber, 2014; Brandalise et al., 2016).

357 We asked whether the effect of the different  
358 stimulation protocols might also be visible in the dendritic  
359  $\text{Ca}^{2+}$  signals, which we previously showed are  
360 associated with the NMDA spikes (Brandalise et al.,  
361 2016). Simultaneous 2PLSM imaging of Fluo-5F in at  
362 least 2 different fields of view (FOVs) ( $\sim 30$  stimulations  
363 each; Fig. 2F; Methods) revealed a negligible fraction of

364 local  $\text{Ca}^{2+}$  transients in coincidence with the paired stim-  
365 ulations during ITDP1 ( $2.2 \pm 0.4\%$ ,  $n = 9$ ; Fig. 1G, H),  
366 whereas such events were readily detected in the same  
367 FOVs during ITDP2 ( $45.6 \pm 4.3\%$ ,  $n = 9$ ; Fig. 2G, H).  
368 The  $\text{Ca}^{2+}$  transients remained confined to single  
369 branches (width:  $13.5 \pm 2.2\ \mu\text{m}$ ,  $n = 9$  cells), and were  
370 detected in at least one of the branches connected to  
371 the recording electrode ( $\Delta F/F = 63 \pm 6\%$ ,  $n = 9$ ;  
372 Fig. 1I) in high coincidence with the supralinear potentials  
373 ( $92.2 \pm 4.5\%$ ,  $n = 9$ ). In accordance with the electric  
374 dendritic recordings, the amplitude of the  $\text{Ca}^{2+}$  transients  
375 increased with the distance from the soma ( $r = 0.61$ ,  
376 Fig. 4D), which supports the notion that NMDA spikes  
377 are generated locally and close to the rCA3 synapses.  
378 Together, this data shows that the reduction of NMDA  
379 channel openings at a segment of the dendritic tree pre-  
380 vents the local onset of NMDA spikes and consequently  
381 the induction of LTP.

### 382 NMDA spikes are independently generated at 383 different branches and induce branch-constrained 384 LTP

385 In a second set of experiments we placed the theta glass  
386 electrode slightly more distal from the dendritic electrode.  
387 We reasoned that this may lead to a strong activation of  
388 more dendritic branches than the one we were  
389 recording from (see schematic in Fig. 3A). Indeed,  
390 stimulation resulted in postsynaptic responses with  
391 lower amplitudes and slower rise times at the dendritic  
392 compartment (green) as compared to the soma (blue)  
393 (Fig. 3B; amplitude:  $3.9 \pm 1.0\text{mV}$  dendrite,  $6.2$   
394  $\pm 1.0\text{mV}$  soma,  $P = 0.01$ ; rise time:  $7.8 \pm 1.0\text{ms}$   
395 dendrite,  $5.7 \pm 0.7\text{ms}$  soma;  $P = 0.007$ ;  $n = 5$ ). This  
396 confirms that the majority of the activated synapses  
397 were on average in closer proximity to the somatic  
398 recording electrode than to the recorded dendritic  
399 compartment.

400 Similar to the first set of experiments, we delivered two  
401 ITDP pairing protocols, the first one while hyperpolarizing  
402 the recorded dendrite with a negative current injection  
403 (ITDP1, Fig. 3C), and a second while leaving the resting  
404 membrane potential unaltered (ITDP2, Fig. 3C). Again,  
405 we reasoned that a local hyperpolarization should  
406 mainly affect the recorded dendrite and to a lesser  
407 extent the rest of the dendritic tree. Hence, because the  
408 majority of the activated rCA3 inputs are presumably  
409 broadly distributed over the dendritic tree, their capacity  
410 to trigger NMDA spikes at other locations should not, or  
411 only slightly, be affected. Consistent with this  
412 hypothesis, during ITDP1, no NMDA spikes were  
413 detected in the recorded dendritic compartment ( $3.7$   
414  $\pm 1.3\%$ ,  $n = 5$ ), whereas a significantly higher number  
415 could be identified through the somatic electrode ( $30.8$   
416  $\pm 4.6\%$ ,  $n = 5$ ,  $P = 0.003$ ). The latter events putatively  
417 originated from branches in parts of the dendritic tree  
418 different from where the recorded compartment was  
419 located. The absence of NMDA spikes at the  
420 hyperpolarized dendritic compartment was not due to a  
421 lack of converging inputs on this segment, since  
422 numerous supralinear events could be detected upon  
423 the omission of the hyperpolarizing step during ITDP2

(Fig. 3C). In fact, ITDP2 evoked a similar number of supralinear events at both the dendritic and somatic compartments ( $57.4 \pm 4.2\%$  for the soma;  $56.1 \pm 3.7\%$  for the dendrite,  $n = 5$ ,  $P = 0.2$ ). Nonetheless, at the soma they had a higher amplitude as compared to those triggered during ITDP1 (from  $7.3 \pm 0.7$  mV to  $10.4 \pm 1.1$  mV,  $P = 0.002$ ,  $n = 5$ , Fig. 3C), presumably due to the summation of the depolarization induced by the NMDA spikes originated at the two different dendritic compartments (FOV1 and FOV2) and converging at the soma.

Upon both ITDP1 and ITDP2, we found a significant increase in the rCA3 EPSPs at the soma (Fig. 3C; ITDP1: from  $5.9 \pm 0.2$  mV to  $7.8 \pm 0.3$  mV,  $P = 0.005$ ,  $n = 5$ ; ITDP2: from  $7.8 \pm 0.3$  mV to  $10.2 \pm 0.9$  mV,  $P = 0.0007$ ,  $n = 5$ ), indicating that LTP had been induced at a broad number of synapses. Interestingly, only a small increase in rCA3 EPSP amplitudes was detected at the dendritic compartment upon ITDP1, but this was statistically non-significant (from  $4.1 \pm 0.4$  mV pre-ITDP1 to  $4.5 \pm 0.1$  mV post-ITDP1,  $P = 0.08$ ,  $n = 5$ ). This increase became statistically significant after release of the local hyperpolarization step during ITDP2 (from  $5.5 \pm 0.1$  mV pre-ITDP2 to  $8.3 \pm 0.5$  mV post-ITDP2,  $P = 0.0003$ ,  $n = 5$ ). Together, this suggests that NMDA spikes generated at various places in the dendritic tree do not readily induce LTP in branches that remain hyperpolarized during the pairing, which is consistent with the NMDAR-dependency of synaptic LTP.

The results of the electrophysiological analysis were confirmed by the  $\text{Ca}^{2+}$  imaging data. Using simultaneous 2PLSM from 2 FOVS (Fig. 3F), we failed to detect dendritic  $\text{Ca}^{2+}$  transients in the recorded dendritic compartment (Fig. 3G, H,  $3.7 \pm 1.2\%$  for FOV1,  $n = 5$ ) but we did detect events on other branches ( $57.8 \pm 9.6\%$ , for FOV2). The  $\text{Ca}^{2+}$  transients in FOV2 had a very high coincidence with the NMDA spikes recorded at the soma ( $89.4 \pm 3.4\%$ ,  $n = 5$ ). Interestingly, the amplitudes of the  $\text{Ca}^{2+}$  transients in FOV2 were not significantly different between ITDP1 and ITDP2 (ITDP1:  $\Delta F/F = 57.2 \pm 12.3\%$ ; ITDP2:  $\Delta F/F = 59.8 \pm 14.2\%$ ,  $P = 0.8$ ,  $n = 5$ ) as well as the spatial spread of the  $\text{Ca}^{2+}$  signal within the branch ( $11.7 \pm 2.4$   $\mu\text{m}$ ,  $P = 0.7$ ,  $n = 5$ ). This demonstrates that the  $\text{Ca}^{2+}$  influx detected at each branch was not propagating or diffusing to the neighboring dendrites. Instead they remained confined to the region where they originated, independently of the numbers of the activated branches.

## DISCUSSION

We investigated the role of localized NMDA spikes in inducing LTP at recurrent synapses of CA3 cells in rat hippocampal slices, using dendritic and somatic patch clamp recordings combined with simultaneous imaging of dendritic  $\text{Ca}^{2+}$  transients. We induced NMDA spikes and LTP using an ITDP protocol that consisted of the repetitive paired stimulation of rCA3 and MF inputs (Brandalise and Gerber, 2014). In this protocol the activa-

tion of MF inputs on the apical trunk (with a 10-ms delay after the rCA3 activation) generates a powerful sub-threshold response that relieves the magnesium block at rCA3 synapses, and thereby acts as a gate for the induction of supralinear NMDA-mediated synaptic responses and LTP at rCA3 synapses (Brandalise and Gerber, 2014). By using focal synaptic stimulation of rCA3 fibers we met the biophysical requirements for inducing NMDA spikes (Schiller et al., 2000), i.e. the activation of a cluster of synapses on a few targeted branches along with the opening of extra-synaptic receptors (Larkum and Nevian, 2008; Chalifoux and Carter, 2011; Kleindienst et al., 2011; Oikonomou et al., 2012). Despite the fact that we could only target primary dendrites with our recording electrodes, the simultaneous use of 2PLSM revealed that the rise of cytosolic  $\text{Ca}^{2+}$ , which is associated with the NMDA spikes, originated preferentially in the thinner, secondary-order dendrites, as previously described (Polisky et al., 2004; Losonczy et al., 2008; Branco et al., 2010). By using a local hyperpolarization step, applied via the dendritic electrode, we prevented the focal stimulation from triggering NMDA spikes along the patch-clamped dendrite, which confirms that the initiation of these spikes depends on local, presumably synaptic mechanisms (Lisman, 2017). The local hyperpolarization also counteracted an increase of rCA3 non-paired synaptic responses, which would normally occur after multiple pairings (Brandalise et al., 2016). This indicates that subthreshold responses *per se* do not induce LTP, which confirms the strong dependency of synaptic plasticity on dSpikes in this paradigm (Brandalise et al., 2016). The absence of a potentiation effect was not due to a lack of synaptic mechanisms for LTP at other locations, since a second ITDP protocol in which hyperpolarization was omitted did evoke LTP. These results did not, however, exclude the possibility that the dendritic hyperpolarization had prevented opening of NMDA receptors on other branches. By moving the stimulation electrode further away from the dendritic recording electrode, we were able to activate synapses located on other branches. This allowed us to test how a local hyperpolarization of one dendritic segment would impact synapses on adjacent branches. In this experiment, the local hyperpolarization did not prevent the generation of NMDA spikes in other branches, as shown by 2PLSM of  $\text{Ca}^{2+}$  events, as well as by the occurrence of supralinear events at the soma. Interestingly, under these conditions LTP could be evoked as measured at the soma, which was likely due to plasticity of synapses at distant locations from the recorded dendrite. Indeed, and not unexpectedly, LTP was not observed at the dendritic compartment that was hyperpolarized. This is in line with the finding that this type of LTP depends on synaptic NMDA receptors (Dudman et al., 2007; Losonczy et al., 2008; Brandalise and Gerber, 2014; Brandalise et al., 2016).

Taken together, our data support the hypothesis that NMDA spikes and their associated  $\text{Ca}^{2+}$  transients can be generated locally in single dendritic branches of CA3 cells (Branco and Häusser, 2010) and that these branch-constrained NMDA spikes can trigger LTP sepa-

544 rately from one another, and thus act as unitary modules  
545 for synaptic plasticity (Branco and Häusser, 2011;  
546 Kastellakis et al., 2015; Mel et al., 2017; Kastellakis and  
547 Poirazi, 2019; Poirazi and Papoutsis, 2020).

548 What is the physiological relevance of this type of  
549 plasticity (Golding et al., 2002; Lisman and Spruston,  
550 2005; Remy and Spruston, 2007)? As argued previously,  
551 the giant synapses of the MF inputs are thought to have a  
552 detonator-like effect on CA3 neurons, which would be  
553 necessary for spike-timing-dependent LTP (Lisman and  
554 Spruston, 2010). However, MF inputs, originating from  
555 sparsely firing dentate granule cells do not readily evoke  
556 long bursts of action potentials *in vivo*, and thus it has  
557 been debated as to whether synapses of the local circuitry  
558 could undergo efficient plasticity (Henze et al., 2002). In  
559 accordance with previous work, we show here that the  
560 strong subthreshold depolarization as induced by MF  
561 inputs allows the generation of local NMDA spikes in more  
562 distal dendrites, which is as powerful or perhaps even  
563 more efficient in inducing LTP than back-propagating  
564 APs (Hardie and Spruston, 2009). Therefore, in behaving  
565 animals, appropriately timed subthreshold MF input could  
566 trigger LTP of theta-timed inputs onto CA3 cells from  
567 neighboring CA3 cells, and provide a framework for hip-  
568 pocampal neuronal ensemble formation that is implicated  
569 in memory. Could the local prevention of dSpike genera-  
570 tion be physiologically relevant? Despite the fact that the  
571 square hyperpolarization step that we applied is highly  
572 artificial, it could mimic the effects of physiological events.  
573 For example, local dendritic inhibition can evoke  
574 compartment-specific hyperpolarization (Murayama  
575 et al., 2009; Dorsett et al., 2021). Such forms of inhibition  
576 may gate the induction of plasticity in protocols where  
577 dSpikes have been observed to be effectors (Cichon  
578 and Gan, 2015; Doron et al., 2017; Williams and  
579 Holtmaat, 2019). Other studies have described an inhibi-  
580 tory effect of somatostatin-expressing interneurons on the  
581 coupling between NMDA spikes and somatic bursting  
582 (Lovett-Barron et al., 2012). Activation of interneurons  
583 can also negatively affect the calcium influx occurring dur-  
584 ing a back-propagating action potential (Müllner et al.,  
585 2015). It is feasible that a similar mechanism is involved  
586 in modulating branch-constrained calcium transients  
587 associated with local NMDA spikes. For instance,  
588 interneurons interneurons targeting the upper cortical  
589 layer (such as Martinotti cells) can control dendritic spikes  
590 on the apical part of the layer 5 pyramidal cells; basket  
591 cells on the contrary are more prone to modulate the cal-  
592 cium spikes occurring in the main trunk of the same pyra-  
593 midal cell (Gidon and Segev, 2012). The local  
594 hyperpolarization could also mimic the activity-  
595 dependent modulation of particular ion channel conduc-  
596 tances at dendritic nodes, which have been shown to  
597 strongly regulate local dSpike generation (Soldado-  
598 Magraner et al., 2020; Humphries et al., 2021).

## UNCITED REFERENCE

599  
600 Pagès et al. (2021).

## DECLARATION OF COMPETING INTEREST

The authors declare that they have no known competing financial interests or personal relationships that could have appeared to influence the work reported in this paper.

## ACKNOWLEDGEMENTS

We thank D. Göckeritz-Dujmovic for the preparation of the organotypic slice cultures preparation, S. Giger and H. Kasper for technical support, and F. David and P. Morciano for IT support. We thank John Lisman for contributing to experimental design, and Beat Gähwiler for discussions of the results.

## AUTHOR CONTRIBUTION

F.B. designed with U.G. the experiments. F.B. performed electrophysiological and calcium imaging experiments and analyzed data. S.C. performed calcium imaging experiments and analyzed data. R.L. analyzed data. F. H. designed experiments. F.B and A.H., U.G. wrote the paper.

## REFERENCES

- Amaral DG, Witter MP (1989) The three-dimensional organization of the hippocampal formation: a review of anatomical data. *Neuroscience* 31(3):571–591.
- Antic SD, Zhou W-L, Moore AR, Short SM, Ikonomu KD (2010) The decade of the dendritic NMDA spike. *J Neurosci Res* 88(14):2991–3001.
- Ariav G, Polsky A, Schiller J (2003) Submillisecond precision of the input-output transformation function mediated by fast sodium dendritic spikes in basal dendrites of CA1 pyramidal neurons. *J Neurosci* 23(21):7750–7758.
- Augustinaite S, Kuhn B, Helm PJ, Heggelund P (2014) NMDA spike/plateau potentials in dendrites of thalamocortical neurons. *J Neurosci* 34(33):10892–10905.
- Basu J, Zaremba JD, Cheung SK, Hitti FL, Zemelman BV, Losonczy A, Siegelbaum SA (2016) Gating of hippocampal activity, plasticity, and memory by entorhinal cortex long-range inhibition. *Science* 351(6269).
- Bono J, Clopath C (2017) Modeling somatic and dendritic spike mediated plasticity at the single neuron and network level. *Nat Commun* 8(1):1–17.
- Branco T, Häusser M (2010) The single dendritic branch as a fundamental functional unit in the nervous system. *Curr Opin Neurobiol* 20(4):494–502.
- Branco T, Clark BA, Häusser M (2010) Dendritic discrimination of temporal input sequences in cortical neurons. *Science* 329(5999):1671–1675.
- Branco T, Häusser M (2011) Synaptic integration gradients in single cortical pyramidal cell dendrites. *Neuron* 69(5):885–892.
- Brandalise F, Gerber U (2014) Mossy fiber-evoked subthreshold responses induce timing-dependent plasticity at hippocampal CA3 recurrent synapses. *Proc Natl Acad Sci U S A* 111(11):4303–4308.
- Brandalise F, Carta S, Helmchen F, Lisman J, Gerber U (2016) Dendritic NMDA spikes are necessary for timing-dependent associative LTP in CA3 pyramidal cells. *Nat Commun* 7(1):1–9.
- Cash S, Yuste R (1998) Input summation by cultured pyramidal neurons is linear and position-independent. *J Neurosci* 18(1):10–15.
- Cash S, Yuste R (1999) Linear summation of excitatory inputs by CA1 pyramidal neurons. *Neuron* 22(2):383–394.

- 661 Chalifoux JR, Carter AG (2011) Glutamate spillover promotes the  
662 generation of NMDA spikes. *J Neurosci* 31(45):16435–16446.
- 663 Cichon J, Gan W-B (2015) Branch-specific dendritic Ca<sup>2+</sup> spikes  
664 cause persistent synaptic plasticity. *Nature* 520(7546):180–185.
- 665 Debanne D, Guerineau NC, Gähwiler BH, Thompson SM (1995)  
666 Physiology and pharmacology of unitary synaptic connections  
667 between pairs of cells in areas CA3 and CA1 of rat hippocampal  
668 slice cultures. *J Neurophysiol* 73(3):1282–1294.
- 669 Doron M, Chindemi G, Muller E, Markram H, Segev I (2017) Timed  
670 synaptic inhibition shapes NMDA spikes, influencing local  
671 dendritic processing and global I/O properties of cortical  
672 neurons. *Cell Rep* 21(6):1550–1561.
- 673 Dorset C, Philpot BD, Smith SL, Smith IT (2021) The impact of SST  
674 and PV interneurons on nonlinear synaptic integration in the  
675 neocortex. *Neuro* 8(5).
- 676 Dudman JT, Tsay D, Siegelbaum SA (2007) A role for synaptic inputs  
677 at distal dendrites: instructive signals for hippocampal long-term  
678 plasticity. *Neuron* 56(5):866–879.
- 679 Gambino F, Pagès S, Kehayas V, Baptista D, Tatti R, Carleton A,  
680 Holtmaat A (2014) Sensory-evoked LTP driven by dendritic  
681 plateau potentials in vivo. *Nature* 515(7525):116–119.
- 682 Gähwiler BH (1981) Organotypic monolayer cultures of nervous  
683 tissue. *J Neurosci Methods* 4(4):329–342.
- 684 Gidon A, Segev I (2012) Principles governing the operation of  
685 synaptic inhibition in dendrites. *Neuron* 75(2):330–341.
- 686 Golding NL, Spruston N (1998) Dendritic sodium spikes are variable  
687 triggers of axonal action potentials in hippocampal CA1 pyramidal  
688 neurons. *Neuron* 21(5):1189–1200.
- 689 Golding NL, Staff NP, Spruston N (2002) Dendritic spikes as a  
690 mechanism for cooperative long-term potentiation. *Nature* 418  
691 (6895):326–331.
- 692 Grienberger C, Chen X, Konnerth A (2014) NMDA receptor-  
693 dependent multidendrite Ca<sup>2+</sup> spikes required for hippocampal  
694 burst firing in vivo. *Neuron* 81(6):1274–1281.
- 695 Hardie J, Spruston N (2009) Synaptic depolarization is more effective  
696 than back-propagating action potentials during induction of  
697 associative long-term potentiation in hippocampal pyramidal  
698 neurons. *J Neurosci* 29(10):3233–3241.
- 699 Hawkins J, Ahmad S (2016) Why neurons have thousands of  
700 synapses, a theory of sequence memory in neocortex. *Front*  
701 *Neural Circuits* 10:23.
- 702 Henze DA, Wittner L, Buzsáki G (2002) Single granule cells reliably  
703 discharge targets in the hippocampal CA3 network in vivo. *Nat*  
704 *Neurosci* 5(8):790–795.
- 705 Humphries R, Mellor J, O'Donnell C (2021) Acetylcholine boosts  
706 dendritic NMDA spikes in a CA3 pyramidal neuron model.  
707 *bioRxiv*..
- 708 Kamiya H, Shinozaki H, Yamamoto C (1996) Activation of  
709 metabotropic glutamate receptor type 2/3 suppresses  
710 transmission at rat hippocampal mossy fibre synapses. *J*  
711 *Physiol* 493(2):447–455.
- 712 Kampa BM, Letzkus JJ, Stuart GJ (2006) Requirement of dendritic  
713 calcium spikes for induction of spike-timing-dependent synaptic  
714 plasticity. *J Physiol* 574(1):283–290.
- 715 Kastellakis G, Cai DJ, Mednick SC, Silva AJ, Poirazi P (2015)  
716 Synaptic clustering within dendrites: an emerging theory of  
717 memory formation. *Prog Neurobiol* 126:19–35.
- 718 Kastellakis G, Poirazi P (2019) Synaptic clustering and memory  
719 formation. *Front Mol Neurosci* 12:300.
- 720 Kim Y, Hsu CL, Cembrowski MS, Mensh BD, Spruston N (2015)  
721 Dendritic sodium spikes are required for long-term potentiation at  
722 distal synapses on hippocampal pyramidal neurons. *Elife* 4  
723 e06414.
- 724 Kleindienst T, Winnubst J, Roth-Alpermann C, Bonhoeffer T,  
725 Lohmann C (2011) Activity-dependent clustering of functional  
726 synaptic inputs on developing hippocampal dendrites. *Neuron* 72  
727 (6):1012–1024.
- 728 Kumar A, Schiff O, Barkai E, Mel BW, Poleg-Polsky A, Schiller J  
729 (2018) NMDA spikes mediate amplification of inputs in the rat  
730 piriform cortex. *Elife*, 7, e38446..
- Langer D, van't Hoff M, Keller AJ, Nagaraja C, Pfäffli OA, Göldi M, 731  
Kasper H, Helmchen F (2013) HelioScan: a software framework 732  
for controlling in vivo microscopy setups with high hardware 733  
flexibility, functional diversity and extendibility. *J Neurosci* 734  
*Methods* 215(1):38–52. 735
- Larkum ME, Nevian T (2008) Synaptic clustering by dendritic 736  
signalling mechanisms. *Curr Opin Neurobiol* 18(3):321–331. 737
- Lisman J (2017) Glutamatergic synapses are structurally and 738  
biochemically complex because of multiple plasticity processes: 739  
long-term potentiation, long-term depression, short-term 740  
potentiation and scaling. *Philos Trans R Society B: Biol Sci* 372  
(1715):20160260. 741
- Lisman J, Spruston N (2005) Postsynaptic depolarization 742  
requirements for LTP and LTD: a critique of spike timing- 743  
dependent plasticity. *Nat Neurosci* 8(7):839–841. 744
- Lisman J, Spruston N (2010) Questions about STDP as a general 745  
model of synaptic plasticity. *Front Synaptic Neurosci* 2:140. 746
- London M, Häusser M (2005) Dendritic computation. *Annu Rev* 747  
*Neurosci* 28(1):503–532. 748
- Losonczy A, Makara JK, Magee JC (2008) Compartmentalized 749  
dendritic plasticity and input feature storage in neurons. *Nature* 750  
452(7186):436–441. 751
- Lovett-Barron M, Turi GF, Kaifosh P, Lee PH, Bolze F, Sun X-H, 752  
Nicoud J-F, Zemelman BV, Sternson SM, Losonczy A (2012) 753  
Regulation of neuronal input transformations by tunable dendritic 754  
inhibition. *Nat Neurosci* 15(3):423–430. 755
- Major G, Larkum ME, Schiller J (2013) Active properties of 756  
neocortical pyramidal neuron dendrites. *Annu Rev Neurosci* 36  
(1):1–24. 757
- Major G, Polsky A, Denk W, Schiller J, Tank DW (2008) 758  
Spatiotemporally graded NMDA spike/plateau potentials in basal 759  
dendrites of neocortical pyramidal neurons. *J Neurophysiol* 99  
(5):2584–2601. 760
- Makara J, Magee J (2013) Variable dendritic integration in 761  
hippocampal CA3 pyramidal neurons. *Neuron* 80(6):1438–1450. 762
- Mel BW, Schiller J, Poirazi P (2017) Synaptic plasticity in dendrites: 763  
complications and coping strategies. *Curr Opin Neurobiol* 764  
43:177–186. 765
- Mori M, Abegg MH, Gähwiler BH, Gerber U (2004) A frequency- 766  
dependent switch from inhibition to excitation in a hippocampal 767  
unitary circuit. *Nature* 431(7007):453–456. 768
- Müllner F, Wierenga C, Bonhoeffer T (2015) Precision of inhibition: 769  
dendritic inhibition by individual GABAergic synapses on 770  
hippocampal pyramidal cells is confined in space and time. 771  
*Neuron* 87(3):576–589. 772
- Murayama M, Pérez-Garci E, Nevian T, Bock T, Senn W, Larkum ME 773  
(2009) Dendritic encoding of sensory stimuli controlled by deep 774  
cortical interneurons. *Nature* 457(7233):1137–1141. 775
- Oikonomou KD, Short SM, Rich MT, Antic SD (2012) Extrasynaptic 776  
glutamate receptor activation as cellular bases for dynamic range 777  
compression in pyramidal neurons. *Front Physiol* 3:334. 778
- Pagès S, Chenouard N, Chéreau R, Kouskoff V, Gambino F, 779  
Holtmaat A (2021) An increase in dendritic plateau potentials is 780  
associated with experience-dependent cortical map 781  
reorganization. *Proc Natl Acad Sci U S A*, 118(9).. 782
- Poirazi P, Papoutsis A (2020) Illuminating dendritic function with 783  
computational models. *Nat Rev Neurosci* 21(6):303–321. 784
- Polsky A, Mel BW, Schiller J (2004) Computational subunits in thin 785  
dendrites of pyramidal cells. *Nat Neurosci* 7(6):621–627. 786
- Rancz EA, Häusser M (2006) Dendritic calcium spikes are tunable 787  
triggers of cannabinoid release and short-term synaptic plasticity 788  
in cerebellar Purkinje neurons. *J Neurosci* 26(20):5428–5437. 789
- Rashid SK, Pedrosa V, Dufour MA, Moore JJ, Chavlis S, Delatorre 790  
RG, Basu J (2020) The dendritic spatial code: branch-specific 791  
place tuning and its experience-dependent decoupling. *bioRxiv*.. 792
- Remy S, Spruston N (2007) Dendritic spikes induce single-burst long- 793  
term potentiation. *Proc Natl Acad Sci U S A* 104  
(43):17192–17197. 794
- Remy S, Csicsvari J, Beck H (2009) Activity-dependent control of 795  
neuronal output by local and global dendritic spike attenuation. 796  
*Neuron* 61(6):906–916. 797

802 Salin PA, Scanziani M, Malenka RC, Nicoll RA (1996) Distinct short- 816  
803 term plasticity at two excitatory synapses in the hippocampus. 817  
804 Proc Natl Acad Sci U S A 93(23):13304–13309. 818  
805 Schiller J, Major G, Koester HJ, Schiller Y (2000) NMDA spikes in 819  
806 basal dendrites of cortical pyramidal neurons. Nature 404 820  
807 (6775):285–289. 821  
808 Sheffield ME, Dombeck DA (2015) Calcium transient prevalence 822  
809 across the dendritic arbour predicts place field properties. Nature 823  
810 517(7533):200–204. 824  
811 Sheffield MEJ, Adoff MD, Dombeck DA (2017) Increased prevalence 825  
812 of calcium transients across the dendritic arbor during place field 826  
813 formation. Neuron 96(2):490–504.e5. 827  
814 Soldado-Magraner S, Brandalise F, Honnuraiah S, Pfeiffer M, 828  
815 Moulinier M, Gerber U, Douglas R (2020) Conditioning by 829  
subthreshold synaptic input changes the intrinsic firing pattern of  
CA3 hippocampal neurons. J Neurophysiol 123(1):90–106.  
Spruston N (2008) Pyramidal neurons: dendritic structure and  
synaptic integration. Nat Rev Neurosci 9(3):206–221.  
Stuart GJ, Spruston N (2015) Dendritic integration: 60 years of  
progress. Nat Neurosci 18(12):1713–1721.  
Suzuki M, Larkum ME (2017) Dendritic calcium spikes are clearly  
detectable at the cortical surface. Nat Commun 8(1):1–11.  
Topolnik L, Camiré O (2019) Non-linear calcium signalling and  
synaptic plasticity in interneurons. Curr Opin Neurobiol  
54:98–103.  
Williams LE, Holtmaat A (2019) Higher-order thalamocortical inputs  
gate synaptic long-term potentiation via disinhibition. Neuron 101  
(1):91–102.e4.

830  
831  
832

(Received 18 March 2021, Accepted 3 October 2021)  
(Available online xxxx)